frontiers in Energy Research

BRIEF RESEARCH REPORT
published: 14 February 2022
doi: 10.3389/fenrg.2021.816454

Preparation of WO_3/Mo/CrNi/TiO_2 Composite Multifunctional Photothermal Conversion Films With Self-Cleaning and Low Emissivity

Wenqing Cheng[1], Huixue Ren[1], Yanxue Chen[2], Daoji Wu[1]*, Shuai Zhang[1], Chunfeng Yu[3] and Fangjun Li[3]*

[1]School of Municipal and Environmental Engineering, Shandong Jianzhu University, Jinan, China, [2]School of Physics, Shandong University, Jinan, China, [3]Shandong Sanqi Energy Co. Ltd., Jinan, China

To improve the sunlight transmittance and infrared reflectivity, different membrane compositions are designed to realize self-cleaning and low emissivity of the membrane. The WO_3/Mo/CrNi/TiO_2 composite film was prepared by magnetron sputtering technology, and the complementary effect of these films with four different argon/oxygen ratios of TiO_2 layer and different film thicknesses was analyzed. The microstructure characterization proves that the self-cleaning function of the composite film is determined by the photocatalytic properties and superhydrophilic properties of the TiO_2.

Keywords: low emissivity, hydrophilicity, self-cleaning, composite films, magnetron sputtering

OPEN ACCESS

Edited by:
Xinqi Chen,
Hubei University of Education, China

Reviewed by:
Wen Zhu,
Huazhong University of Science and Technology, China
Adisorn Buranawong,
Burapha University, Thailand

****Correspondence:***
Huixue Ren
renhx138@163.com
Daoji Wu
wdj@sdjzu.edu.cn

Specialty section:
This article was submitted to Electrochemical Energy Conversion and Storage, a section of the journal Frontiers in Energy Research

Received: *16 November 2021*
Accepted: *23 December 2021*
Published: *14 February 2022*

Citation:
Cheng W, Ren H, Chen Y, Wu D, Zhang S, Yu C and Li F (2022) Preparation of WO_3/Mo/CrNi/TiO_2 Composite Multifunctional Photothermal Conversion Films With Self-Cleaning and Low Emissivity. Front. Energy Res. 9:816454. doi: 10.3389/fenrg.2021.816454

INTRODUCTION

Solar energy is a continuous source of renewable energy. Human beings mainly live by the thermal radiation provided by the sun. For ordinary glass, more than 89% of the infrared emissive energy is absorbed by the glass, resulting in the rise of the glass temperature, and then a large amount of heat is dissipated through the heat exchange between the glass and the surrounding air, resulting in a large amount of outdoor heat brought by sunlight entering the room or a large part of indoor heat escaping to the outside (Granqvist, 2007; Dalapati et al., 2018). These conditions have seriously increased the burden of air conditioning and wasted a lot of energy. In the standard atmospheric spectrum, the energy in ultraviolet, visible, and infrared bands accounts for about 3, 44, and 53% of the total solar radiation energy, respectively. Based on the standard atmospheric spectral radiation energy distribution, the ideal solar insulation film is able to completely reflect 0.3–0.38 μm ultraviolet light, transmitted 0.38–0.78 μm visible light, and well reflected 0.78–2.5 μm infrared light. In the standard atmospheric spectrum, most of the heat radiated to the surface of earth is concentrated in 0.78–2.5 μm infrared band. Although the radiant heat in the visible light band of the range of 0.38–0.78 μm is also large, to ensure sufficient visible light indoors or in the vehicle, its transmittance in the visible light region is generally controlled at 70–80%. In daily life, solar insulation film can protect indoor or car objects and people from ultraviolet radiation by isolating ultraviolet light, prolong the aging of indoor objects, and reduce glare by adjusting the intensity of visible light entering the car, effectively avoiding traffic accidents. The composite film is an engineering film that can prevent ultraviolet light, adjust the visible light entering the room or vehicle, and well prevent infrared thermal radiation (Frank et al., 1981).

TABLE 1 | Deposition conditions of each layer to produce the multilayer film

Film composition		TiO_2	NiCr	Mo	WO_3
Working power (W)		**150**	**50**	**50**	**50**
Sputtering pressure (Pa)		**1.5**	**0.5**	**0.5**	**1.5**
A	Time (s)	3,600	4	3	1,800
	Thickness (nm)	62.68	4.8	3.4	297.5
	Ar:O_2	2:1	Pure Ar	Pure Ar	3:1
B	Time (s)	1,800	4	5	1,800
	Thickness (nm)	40.2	4.8	6.73	297.5
	Ar:O_2	2:1	Pure Ar	Pure Ar	3:1
C	Time (s)	3,600	4	5	1,800
	Thickness (nm)	62.68	4.8	6.73	297.5
	Ar:O_2	2:1	Pure Ar	Pure Ar	3:1
D	Time (s)	3,600	4	45	1,800
	Thickness (nm)	62.68	4.8	36.3	297.5
	Ar:O_2	2:1	pure Ar	pure Ar	3:1
E	Time (s)	3,600	4	70	1,800
	Thickness (nm)	62.68	4.8	49.54	297.5
	Ar:O_2	2:1	Pure Ar	Pure Ar	3:1
F	Time (s)	3,600	4	95	1,800
	Thickness (nm)	62.68	4.8	59.52	297.5
	Ar:O_2	2:1	Pure Ar	Pure Ar	3:1
TiO_2 layer with argon/oxygen ratio of 1:1	Time (s)	3,600	4	3	1,800
	Thickness (nm)	62.68	4.8	6.4	297.5
	Ar:O_2	1:1	Pure Ar	Pure Ar	3:1
TiO_2 layer with argon/oxygen ratio of 2:1	Time (s)	3,600	4	3	1,800
	Thickness (nm)	62.68	4.8	6.4	297.5
	Ar:O_2	2:1	Pure Ar	Pure Ar	3:1
TiO_2 layer with argon/oxygen ratio of 3:1	Time (s)	3,600	4	3	1,800
	Thickness (nm)	62.68	4.8	6.4	297.5
	Ar:O_2	3:1	Pure Ar	Pure Ar	3:1
TiO_2 layer with argon/oxygen ratio of 4:1	Time(s)	3,600	4	3	1,800
	Thickness (nm)	62.68	4.8	6.4	297.5
	Ar:O_2	4:1	Pure Ar	Pure Ar	3:1

The self-cleaning, hydrophilicity, and low-emissivity properties are very useful in the application as architectural window and automotive glazing. The self-cleaning behavior of a solid surface refers to its ability to remove pollutants under natural conditions. On a hydrophilic surface [water contact angle (WCA) <90°], water forms a thin sheet and washes away impurities, whereas on a hydrophobic surface (WCA >90°), water droplets roll on the surface. However, hydrophilic materials are generally vulnerable to organic compounds, especially compounds with polar functional groups. Hence, to overcome this problem, surface-coated glass is endowed with hydrophilic and photocatalytic properties (Oladipo et al., 2019); thus, the self-cleaning behavior of surface-coated glass becomes more prominent.

At present, the common preparation methods are chemical bath deposition, hydrothermal method, magnetron sputtering, and so on. Physical magnetron sputtering technology has attracted extensive attention due to its advantages of simple process, strong adhesion of film layer, and large area coating (Gong et al., 2019; Gudmundsson, 2020). Sputtering multifunctional film material can not only improve infrared reflectivity but also has the effect of reflection reduction and self-cleaning.

According to the needs of low emissivity, we designed the WO_3/Mo/NiCr/TiO_2 multifunctional film structure, determined an optimized thickness and antireflection characteristics to enhance the visible transmittance, and carried out specific characterization analysis from the aspects of low emissivity and self-cleaning. Otherwise, we investigated the effect of TiO_2 film with different argon oxygen ratios on photocatalysis.

Method

The soda-lime glass with 300 × 300 mm^2 area was applied as the substrates. WO_3/Mo/NiCr/TiO_2 multilayer film was deposited using direct-current magnetron sputtering system in Ar (99.99%) atmosphere. Before deposition, the glass substrates were sequentially ultrasonically cleaned with a detergent solution, deionized water, acetone, and alcohol. Before sputtering, the base pressure of the sputtering chamber was pumped down to 10×10^{-5} Pa by a turbo molecular pump, and the target was pre-sputtered in pure argon for 4 min to remove contaminants on the target surface. The deposition conditions of each layer for samples of different film thicknesses (samples a–f), and TiO_2 layer with four different argon/oxygen ratios of 1:1, 2:1, 3:1, and 4:1 are listed in **Table 1**.

The surface morphology of the thin films was investigated by field-emission scanning electron microscopy (FESEM; ZEISS GeminiSEM300). The crystal structures of the thin films were examined by X-ray diffraction (XRD) with Rigaku X-ray

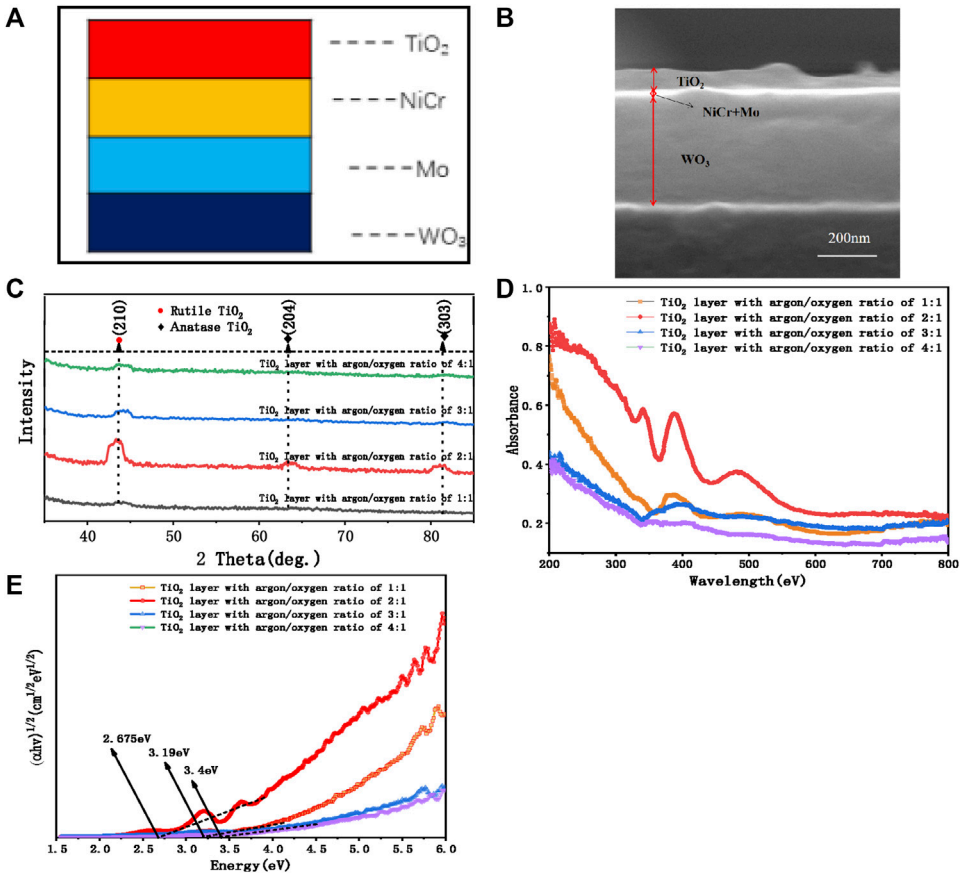

FIGURE 1 | (A) Multifunctional membrane layer structure, **(B)** FESEM image of a membrane layer structure, **(C)** XRD patterns, **(D)** absorption spectra, and **(E)** Tanc's plot for multifunctional membrane of TiO_2 layer with different argon oxygen ratios.

diffractometer under Cu-Kα radiation (1.5406 Å) at 2θ = 30–90°. The surface roughness of the films was measured by atomic force microscopy (AFM; NT-MDT solverp47). The optical transmittance, reflection, and absorbance spectra of the films were recorded by a UV–vis–NIR spectrophotometer (Agilent Cary3500). The hydrophilic properties of the films were evaluated by measuring their water contact angles (WCAs) using a contact angle measuring instrument (KRUSS DSA25). The photocatalytic activities of the thin films were investigated by measuring the degree of decomposition of methylene blue in a glass beaker (50 ml of MB solution, 10 mg/L) under visible light illumination for 2 h. The photocatalytic degradation efficiency of MB was evaluated using the following equation, according to the decrease in the absorption intensity of MB at 664 nm using the following equation:

$$MB\ \ degradation\ \ efficiency = \left(\frac{C_0 - C_t}{C_0}\right) \times 100\%, \quad (1)$$

where C_0 is the initial concentration of the MB solution and C_t is the concentration of the MB solution under visible light irradiation at time t.

RESULT AND DISCUSSION

The structure of the multifunctional membrane layer is shown in **Figure 1A, B**. The outermost layer of TiO_2 has photocatalytic performance and hydrophilicity. This layer mainly provides self-cleaning and photocatalytic function, and prevents the covering of external impurities and dust from affecting the absorption of sunlight by the film layer. Being placed in the outermost layer can also effectively improve the absorption range of visible light. NiCr alloy with better mechanical properties, as the barrier layer, which has good chemical resistance, can prevent the Mo layer from oxidation corrosion at high temperature, guaranteeing the stability of Mo layer and playing its role. Mo layer, as an infrared reflector, increases the range of visible light transmittance and infrared emissivity in the range of the rate, and Mo is hard and tough, has high thermal conductivity, and can effectively improve the use efficiency of solar energy. Mo is easy to be corroded by oxygen in the air, which affects its function of reflecting infrared spectrum; therefore, a dielectric layer should be added on both sides of the Mo layer for protection. Considering the refractive index and stability at high temperature, TiO_2 with high refractive index and stable performance can be selected as

the dielectric layer. It not only has small absorption of visible light but also can absorb, scatter, or reflect a large amount of ultraviolet rays harmful to people and objects. At the same time, to prevent corrosion of Mo layer caused by oxygen and other substances at high temperature, tungsten trioxide, an N-type semiconductor metal oxide that has stable properties and excellent photoelectric conversion performance and photocorrosion resistance, can make more effective use of solar radiation energy (Álvarez-Fraga et al., 2014; Lelis et al., 2019; Firat, 2021).

Effect of Oxygen Partial Pressure and Thickness of TiO_2 on Photocatalysis

The crystal structures of the thin films detected by XRD are shown in **Figure 1C**. The characteristic diffraction peaks of the (210) typical crystal plane of rutile phase appear in TiO_2 films with four different argon/oxygen ratios of 1:1, 2:1, 3:1, and 4:1 (samples g–j), among which the diffraction peak of TiO_2 film with argon/oxygen ratio of 2:1 was the most obvious. The TiO_2 diffraction peaks (204) and (303) of anatase phase also appeared in the TiO_2 film XRD pattern with argon/oxygen ratio of 2:1, and the weak (303) diffraction peak appeared in the TiO_2 film XRD pattern with argon/oxygen ratio of 3:1 and 4:1. However, there was no anatase diffraction peak in the TiO_2 film XRD spectrum of 1:1 argon/oxygen ratio. On the one hand, sputtered metal particles could have more opportunities to fully react with oxygen ions to produce stoichiometric oxides and reduce the appearance of oxide films with intermediate chemical valence. On the other hand, the sufficient reaction with oxygen ions enabled the deposited particles to have sufficient relaxation time to exchange their own energy to the lowest energy position after reaching the substrate surface, resulting in lower XRD diffraction intensity. When the argon/oxygen ratio was higher than a critical value, the target surface would be poisoned and be covered by an oxide layer.

Absorption is one of the most important indexes to evaluate the light utilization efficiency of photocatalysts. The absorptivity of the thin films was analyzed by UV–vis spectroscopy in the wavelength range of 200–800 nm, and their optical bandgaps were calculated according to the following equation (Tauc, 1966):

$$\alpha h\nu = A\left(h\nu - E_g\right)^{n/2} \tag{2}$$

where α, ν, E_g, and A are the absorption coefficient, the optical frequency, the bandgap energy, and a constant, respectively. **Figure 1D** shows the absorbance spectra of films with different TiO_2 argon/oxygen ratios. In the ultraviolet and visible wavelength range, 2:1 film had the highest light absorption rate, followed by the film with 1:1 film. According to **Eq. 2**, the band gap can be estimated by calculating the intercept (Loka and Lee, 2021). According to **Figure 1E**, the band gap of the 2:1 film is 2.68 eV and that of other films is over 3.1 eV (Ahn et al., 2007), whereas that of pure TiO_2 is 3.0–3.2 eV. It is observable that fine crystalline structures reduced the band gap and increased the absorption wavelength range. During photocatalytic degradation, the degradation efficiency of the composite films was higher than that of the pure WO_3 film, indicating that the TiO_2/WO_3 composite films followed a type-II electron transfer mechanism. The holes of WO_3 are transferred to the TiO_2 valence band, and the electrons move from the TiO_2 conduction band to the WO_3 conduction band, improving the redox capacity of the catalyst and conducing the separation of electrons and holes (Kim et al., 2015). In addition, Mo and NiCr in the catalyst could produce free electrons due to the LSPR effect, and these free electrons were transferred to the conduction bands of WO_3 to promote interfacial electron transfer.

It is noticeable from **Figure 2A** that the concentration of MB decreased continuously with the increase of reaction time under ultraviolet and visible light irradiation; thus, compound functional groups of MB were degraded (Mageshwari et al., 2013). After 2 h of reaction, the degradation rate of 2:1 film reached over 93.1%, whereas those of 3:1 and 4:1 film reached 83.2 and 81.3%. The degradation rate was affected by the band gap and crystallization of films. Similarly, for different thicknesses of TiO_2 layer (**Figure 2B**), degradation rate of TiO_2 layers sputtered in 3,600 s (sample a) was highest, and that of the film sputtered in 1,800 s (sample b) was 84.3%. As can be seen from **Figure 2C–F**, the roughness of sample a was the largest, which was due to the formation of metal oxides and the tendency of metal grains to agglomerate, resulting in grain stacking and roughness increase. The contact area is one of the factors determining the photocatalytic efficiency. Higher roughness is conducive to the increase of the contact area, which means that the catalyst has more active sites available for photocatalysis.

Effect of Thickness of TiO_2 on Hydrophilicity

The main mechanism of self-cleaning is as follows: 1) under the irradiation of sunlight, organic pollutants are degraded due to the photocatalytic action of nano-TiO_2; 2) the photoinduced superhydrophilicity of nano-TiO_2 makes the water spread almost completely on the surface of the substrate, separating the pollutants from the substrate, and the pollutants will be taken away with the spread of the water film (Saraswati et al., 2019; Wang et al., 2019).

A well-distributed pore structure is formed on the surface. The surface area and roughness of the film surface are increased by improving the micromorphology of the material surface, so as to achieve the effect of hydrophilicity. As mentioned previously, the roughness of sample c was very large. When the liquid is in contact with a material containing a fine gap, in the case of infiltration, the liquid infiltrates or rises along the gap. The thinner the gap, the higher the rise of the liquid, which means liquid rises on the inner side of the thin tubular material due to the difference of cohesion and adhesion to overcome the gravity.

The characterization of cleaning performance is shown in **Figure 3A**. Because of the high proportion of TiO_2 in the film composition of sample c, the WCA was the smallest, showing the self-cleaning performance of hydrophilic type. The surface of sample c has a multi-dimensional pore structure, which

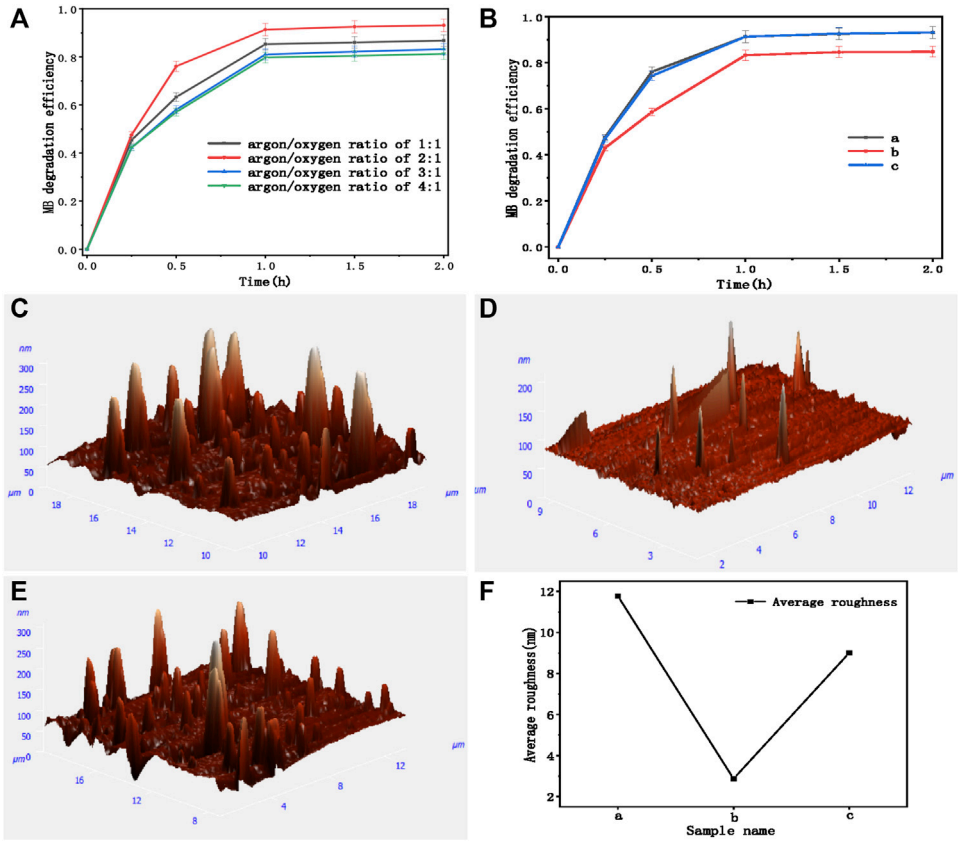

FIGURE 2 | Photocatalytic degradation of methylene blue by multifunctional films **(A)** of TiO_2 layer with different argon oxygen ratios and **(B)** with different layer thicknesses. **(C–F)** AFM images and average roughness of samples a, b, and c (different samples divided by sputtering time; a = 1800sWO$_3$,3sMo,4sNiCr,3600sTiO$_2$; b = 1800sWO$_3$,5sMo,4s,NiCr,1800sTiO$_2$; c = 1800sWO$_3$,5sMo,4sNiCr,3600sTiO$_2$; d = 1800sWO$_3$,45sMo,4sNiCr,3600sTiO$_2$; e = 1800sWO$_3$,70sMo,4sNiCr,3600sTiO$_2$, f = 1800sWO$_3$,95sMo,4sNiCr,3600sTiO$_2$).

means that there will be large protrusions on the surface of the material, and a large number of small protrusions are distributed on each surface of protrusions. The pore size of different dimensions on the surface of sample c is less than its capillary height. Based on the capillary action, water droplets can infiltrate the surface of sample c, and the small holes on the large holes can further promote the infiltration and spreading of water. So, sample c has the best hydrophilicity than others.

Effect of Thickness of High Ultraviolet Reflection Layer on Optical Properties

As shown in **Figure 3C**, when the deposition time of TiO_2 was 3,600 s, the reflectivity of the low-emissivity film in the visible region was the lowest. This is because the thickness of TiO_2 with 3,600-s deposition time might conform to that the spectrum of the optical path difference between the reflected light on its upper surface and lower surface is λ/2, so as to reduce reflection and increase spectral transmittance. When the deposition time of TiO_2 was 1,800 s, the transmittance of low-emissivity film in near infrared was the lowest. According to the spectral analysis of the low-emissivity film in the ultraviolet, visible, and infrared regions, the suitable deposition time of TiO_2 was 1,800 s. The low-emissivity film with this thickness can meet the requirements of low-emissivity film and high infrared reflectivity.

The refractive index of a thin film depends on its density, and its relationship is shown in the following formula (Shen et al., 2008):

$$n = \rho n_s + (1 - \rho) n_v, \tag{3}$$

where n_s and n_v are the refractive indices of solid of the film and the voids, and ρ is the film density. With the rise of the thickness of TiO_2 layer, the migration energy and binding energy of particles on the glass surface increased, the binding between particles was strengthened, the number of pores in the films was reduced, the film density increased, and the refractive index became larger. The amorphous components and porosity of the film decreased and the density increased with the increase of the thickness and time (Ma et al., 2021). The reflectivity, refractive index, and incident angle of the films were calculated according to the Fresnel formula:

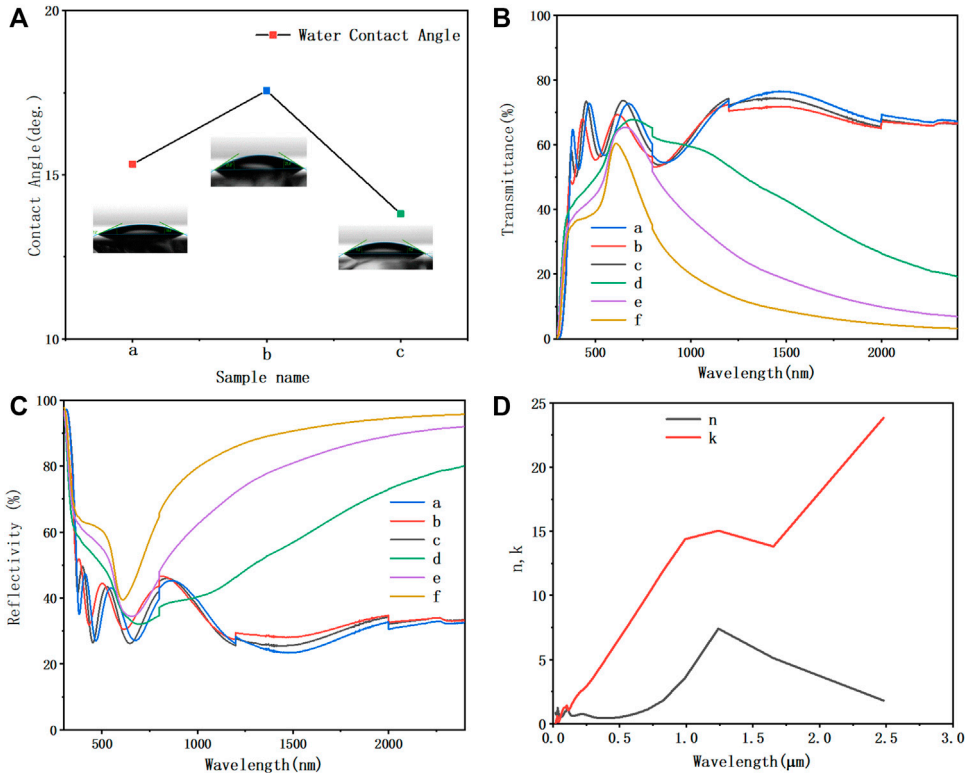

FIGURE 3 | (A) Contact angles for water with different film thicknesses. **(B)** Reflectivity and **(C)** transmittance of multifunctional films with different film thicknesses. **(D)** Curves of refractive index n and extinction coefficient k of metal Mo with wavelength (different samples divided by sputtering time; a = 1800sWO$_3$,3sMo,4sNiCr,3600sTiO$_2$; b = 1800sWO$_3$,5sMo,4s,NiCr,1800sTiO$_2$; c = 1800sWO$_3$,5sMo,4sNiCr,3600sTiO$_2$; d = 1800sWO$_3$,45sMo,4sNiCr,3600sTiO$_2$; e = 1800sWO$_3$,70sMo,4sNiCr,3600sTiO$_2$; f = 1800sWO$_3$,95sMo,4sNiCr,3600sTiO$_2$).

$$R_s = \left[\frac{n_1 \cos\theta_i - \sqrt{n_2^2 - n_1^2 \sin^2\theta_i}}{n_1 \cos\theta_i + \sqrt{n_2^2 - n_1^2 \sin^2\theta_i}}\right]^2 \quad (4)$$

$$R_p = \left[\frac{n_1^2 \cos\theta_i - n_1\sqrt{n_2^2 - n_1^2 \sin^2\theta_i}}{n_1^2 \cos\theta_i + n_1\sqrt{n_2^2 - n_1^2 \sin^2\theta_i}}\right]^2 \quad (5)$$

where R_s and R_p correspond to the refractive indices of s polarization and p polarization, respectively; n_1 and n_2 are the vacuum refractive indices of the first and second media, respectively; and θ_i is the incident angle. According to **Eqs 4**, **5**, the reflectivity of the films was positively correlated with their refractive indices at the same incident angle. Therefore, reflectivity increased with the increase of the thickness of TiO_2 layer.

Effect of Thickness of High Visible Transmittance Layer and High Infrared Reflection Layer on Optical Properties

As mentioned in **Table 1**, the sputtering time of infrared reflection layer (metal Mo layer) of samples a, c, d, e, and f were 3, 5, 45, 70, and 95 s, respectively. It can be seen from **Figure 3B** that the Mo layer with 5-s sputtering time significantly improved the transmittance in the visible light range, and reduced the reflectivity in the visible light range. The average transmittance in the visible region was about 68%. With the sputtering time increased significantly, the thickness of Mo improved the reflectivity in the infrared light region and enhanced the thermal insulation performance. The Mo layer with 95-s sputtering time has the largest infrared reflectivity and the lowest infrared transmittance, but its visible light transmittance decreases. Compared with other samples, the visible light transmittance of sample e (Mo layer with 70-s sputtering time) was about 64%, and the infrared transmittance was 20%. The thin metal layer thickness means low cost. So, sample e has lower economic cost and competitiveness. A longer sputtering time can increase the surface roughness of Mo thin film, leading to an increase of light absorbance (Wen et al., 2012). It suggests that the Mo layer sputtered in 70 s has a combinative advantage to meet the optimal condition of optical properties because of an absorption threshold or continuous film limitation.

The refractive index n and extinction coefficient k parameters of metal Mo layer are shown in **Figure 3D** (Werner et al., 2009). According to the Fresnel formula, with the increase of mental Mo thickness, the reflectivity of infrared region increases and the transmittance decreases. The thickness of Mo layer for sample b and c films is only 6.73nm, so the infrared transmittance is about

30% (**Figure 3C**). After the calculation, increasing the thickness of Mo layer can significantly improve the reflectivity in the infrared region of the films. This is because the thickness of Mo deposition time might conform to that the spectrum of the optical path difference between the reflected light on its upper surface and lower surface is λ/2, so as to the near infrared region curve decreases significantly when the thickness of Mo layer is greater than 10 nm.

According to Bruggeman's aggregation microstructure theory (Bruggeman, 1935), with the increase of the volume fraction of metal particles in the film, the band gap width of the film gradually decreases, and the absorption capacity of light will increase. Due to the relatively large metal thickness, the band gap of sample c is small. With the increase of thickness of Mo layer, more long wave light will be absorbed and short wave light will be reflected, which explains that the absorption of infrared light with wavelength more than 1,000 nm is enhanced when the sputtering time of metal Mo increases from 3 to 95 s. The conductivity will also increase relatively with the increase of metal volume fraction, and the metal characteristics of the film layer will enhance, resulting in the reduction of the reflectance at the long wave, and more light will be transmitted. Therefore, the reflection of the film system to the visible region and the near-infrared region less than 1000 nm is enhanced.

CONCLUSION

In the present study, the WO_3/Mo/CrNi/TiO_2 composite film with different thicknesses and TiO_2 layer with different argon oxygen ratios was prepared by magnetron sputtering technology. The crystallization effect of TiO_2 layer with argon oxygen ratio of 2:1 is the best and the band gap is the smallest, so the degradation efficiency of MB is the highest. The best photocatalytic effect and hydrophilicity is the thin film with TiO_2 layer thickness of 3,600-s deposition time affected by roughness. Mo layer with 5-s sputtering time significantly improves the transmittance in the visible light range. Compared with other samples, the visible light transmittance of sample e was about 64%, the infrared transmittance was 20%, and the cost was lower. According to the spectral analysis of the low-emissivity film in the ultraviolet, visible, and infrared regions, the suitable deposition time of TiO_2 is 1,800 s. Therefore, this study provides new possibilities for the preparation of low infrared transmittance and self-cleaning thin films.

DATA AVAILABILITY STATEMENT

The original contributions presented in the study are included in the article/supplementary material; further inquiries can be directed to the corresponding authors.

AUTHOR CONTRIBUTIONS

WC: conceptualization, methodology, writing—original draft. HR: acquisition, methodology, writing–review and editing. YC: investigation, formal analysis, supervision. DW: validation, visualization. SZ: investigation, supervision. CY: supervision, validation. FL: validation, visualization.

FUNDING

The work was financially supported by Shandong Provincial Major Scientific and Technological Innovation Project (MSTIP) (2019JZZY020211, 2020CXGC011203) and the Natural Science Foundation of Shandong Province (ZR202102280483).

REFERENCES

Ahn, K.-S., Lee, S.-H., Dillon, A. C., Tracy, C. E., and Pitts, R. (2007). The Effect of thermal Annealing on Photoelectrochemical Responses of WO3 Thin Films. *J. Appl. Phys.* 101, 093524. doi:10.1063/1.2729472

Álvarez-Fraga, L., Monclús, M. A., Molina-Aldareguía, J. M., Sánchez-García, J. A., Céspedes, E., Escobar-Galindo, R., et al. (2014). Influence of the IR-Mirror Layer Composition in the Mechanical Properties of Solar Selective Coatings Made from Mo:Si3N4 Cermet. *Thin Solid Films* 571, 316–320. doi:10.1016/j.tsf.2014.05.069

Bruggeman, D. A. G. (1935). Berechnung verschiedener physikalischer Konstanten von heterogenen Substanzen. I. Dielektrizitätskonstanten und Leitfähigkeiten der Mischkörper aus isotropen Substanzen. *Ann. Phys.* 416, 665–679. doi:10.1002/andp.19354160802

Dalapati, G. K., Kushwaha, A. K., Sharma, M., Suresh, V., Shannigrahi, S., and Zhuk, S. (2018). Transparent Heat Regulating (THR) Materials and Coatings for Energy Saving Window Applications: Impact of Materials Design, Micro-Structural, and Interface Quality on the THR Performance. *Prog. Mater. Sci* 95, 42–131. doi:10.1016/j.pmatsci.2018.02.007

Firat, Y. E. (2021). Pseudocapacitive Energy Storage Properties of rGO-WO3 Electrode Synthesized by Electrodeposition. *Mater. Sci. Semiconduct. Process.* 133, 105938. doi:10.1016/J.MSSP.2021.105938

Frank, G., Kauer, E., and Köstlin, H. (1981). Transparent Heat-Reflecting Coatings Based on Highly Doped Semiconductors. *Thin Solid Films* 77, 107–118. doi:10.1016/0040-6090(81)90365-5

Gong, C., Xiao, J., Zhu, L., Qi, M., and Ma, S. (2019). Crystal Structure and Tribological Properties of Molybdenum Disulfide Films Prepared by Magnetron Sputtering Technology. *Curr. Appl. Phys.* 19, 1318–1324. doi:10.1016/j.cap.2019.08.017

Granqvist, C. G. (2007). Transparent Conductors as Solar Energy Materials: A Panoramic Review. *Sol. Energy Mater. Sol. Cells* 91, 1529–1598. doi:10.1016/j.solmat.2007.04.031

Gudmundsson, J. T. (2020). Physics and Technology of Magnetron Sputtering Discharges. *Plasma Sourc. Sci. Technol.* 29, 113001. doi:10.1088/1361-6595/abb7bd

Kim, H.-M., Kim, D., and Kim, B. (2015). Photoinduced Hydrophilicity of TiO2/WO3 Double Layer Films. *Surf. Coat. Techn.* 271, 18–21. doi:10.1016/j.surfcoat.2015.01.054

Lelis, M., Tuckute, S., Varnagiris, S., Urbonavicius, M., Laukaitis, G., and Bockute, K. (2019). Tailoring of TiO2 Film Microstructure by Pulsed-DC and RF Magnetron Co-sputtering. *Surf. Coat. Techn.* 377, 124906. doi:10.1016/j.surfcoat.2019.124906

Loka, C., and Lee, K.-S. (2021). Preparation and Photocatalytic Performance of Silver Nanocrystals Loaded Cu2O-WO3 Composite Thin Films for Visible Light-Active Photocatalysis. *Mater. Res. Bull.* 137, 111192. doi:10.1016/j.materresbull.2020.111192

Ma, C., Wang, L., Fan, X., and Liu, J. (2021). Broadband Antireflection and Hydrophobic CaF2 Film Prepared with Magnetron Sputtering. *Appl. Surf. Sci.* 560, 149924. doi:10.1016/j.apsusc.2021.149924

Mageshwari, K., Mali, S. S., Sathyamoorthy, R., and Patil, P. S. (2013). Template-free Synthesis of MgO Nanoparticles for Effective Photocatalytic Applications. *Powder Techn.* 249, 456–462. doi:10.1016/j.powtec.2013.09.016

Oladipo, H., Garlisi, C., Al-Ali, K., Azar, E., and Palmisano, G. (2019). Combined Photocatalytic Properties and Energy Efficiency via Multifunctional Glass. *J. Environ. Chem. Eng.* 7, 102980. doi:10.1016/j.jece.2019.102980

Saraswati, M., Permadani, R. L., and Slamet, A. (2019). The Innovation of Antimicrobial and Self-Cleaning Using Ag/TiO2 Nanocomposite Coated on Cotton Fabric for Footwear Application. *IOP Conf. Ser. Mater. Sci. Eng.* 509, 012091. doi:10.1088/1757-899X/509/1/012091

Shen, Y., Yu, H., Yao, J., Shao, S., Fan, Z., He, H., et al. (2008). Investigation on Properties of TiO2 Thin Films Deposited at Different Oxygen Pressures. *Opt. Laser Techn.* 40, 550–554. doi:10.1016/j.optlastec.2007.09.003

Tauc, J. (1966). Optical Properties and Electronic Structure of Amorphous Germanium. *Phys. Status Solidi* 3, 37–46. doi:10.1002/pssb.19660150224

Wang, Z., Feng, P., Chen, H., and Yu, Q. (2019). Photocatalytic Performance and Dispersion Stability of Nanodispersed TiO2 Hydrosol in Electrolyte Solutions with Different Cations. *J. Environ. Sci. (China)* 88, 59–71. doi:10.1016/j.jes.2019.07.013

Wen, Z., Tong, D., Xu, J., Yong, L., and Jian, M. (2012). Multifunctional Composite Multilayer Coatings on Glass with Self-Cleaning, Hydrophilicity and Heat-Insulating Properties. *Thin Solid Films* 526, 201–211. doi:10.1016/j.tsf.2012.11.015

Werner, W. S. M., Glantschnig, K., and Ambrosch-Draxl, C. (2009). Optical Constants and Inelastic Electron-Scattering Data for 17 Elemental Metals. *J. Phys. Chem. Ref. Data* 38, 1013–1092. doi:10.1063/1.3243762

Conflict of Interest: Authors CY and FL were employed by Shandong Sanqi Energy Co. Ltd.

The remaining authors declare that the research was conducted in the absence of any commercial or financial relationships that could be construed as a potential conflict of interest.

Publisher's Note: All claims expressed in this article are solely those of the authors and do not necessarily represent those of their affiliated organizations, or those of the publisher, the editors, and the reviewers. Any product that may be evaluated in this article, or claim that may be made by its manufacturer, is not guaranteed or endorsed by the publisher.